



## Investigation of Microstructure And Mechanical Properties of SrBr<sub>2</sub>-doped Calcium Phosphate Materials Produced by Sol-Gel Method

### Sol-jel Yöntemi İle Üretilen SrBr<sub>2</sub> Katkılı Kalsiyum Fosfat Malzemelerin Mikroyapı ve Mekanik Özelliklerinin İncelenmesi

Mehtap Demirel<sup>1\*</sup> , Dilek Çanakçı<sup>1</sup> 

<sup>1</sup> Adiyaman University, Vocational School of Technical Sci, , 02040, Adiyaman, TURKEY

Sorumlu Yazar / Corresponding Author \*: [mdemirel@adiyaman.edu.tr](mailto:mdemirel@adiyaman.edu.tr)

Geliş Tarihi / Received: 06.01.2019

DOI:10.21205/deufmd.2019216224

Kabul Tarihi / Accepted: 21.02.2019

Araştırma Makalesi/Research Article

*Atıf şekli/How to cite: DEMİREL, M., ÇANAKÇI, D. (2019). Investigation of Microstructure And Mechanical Properties of SrBr<sub>2</sub>-doped Calcium Phosphate Materials Produced by Sol-Gel Method. DEUFMD, 21(62), 607-620.*

#### Öz

Bu çalışmada, kalsiyum fosfat esaslı SrBr<sub>2</sub> katkılı sentez malzemeleri sol jel yöntemi ile üretilmiştir. Üretilen malzemelerin morfolojik yapısı ve mekanik özellikleri üzerine SrBr<sub>2</sub> bileşiğinin etkileri incelenmiştir. Bu amaçlar doğrultusunda, biyogreftlerin morfolojik etkileri FTIR, XRD ve SEM-EDX analizleri ile incelenirken, mekanik özellikleri de sertlik ve basma testleri yapılarak araştırılmıştır.

Bütün sentez malzemelerinin üzerine yapılan FTIR ve XRD incelemeleri sonucu, biyogreftler de katkı malzemelerinin kristaliteyi düşürdüğü ve HA(Hidroksiapatit), β-TCP (Beta trikalsiyum fosfat), Ca<sub>3</sub>(Si<sub>3</sub>O<sub>9</sub>), Ca<sub>2</sub>H<sub>4</sub>O<sub>9</sub>P<sub>2</sub> faz yapılarını oluşturduğu gözlenmiştir. Ayrıca yapılan SEM-EDX ve mekanik testler sonucu da, bütün sentez malzemelerinde farklı boyutlarda tane yapısının oluştuğu ve SrBr<sub>2</sub> katkı malzemesinin basma mukavemeti ve sertlik değerlerini yükselttiği belirlenmiştir.

**Anahtar Kelimeler:** Kalsiyum fosfat, SrBr<sub>2</sub>, Sol jel, Mekanik özellikler

#### Abstract

In this study, calcium phosphate based SrBr<sub>2</sub>-doped synthesized materials were produced by sol gel method. The effects of SrBr<sub>2</sub> compound on the morphological structure and mechanical properties of the produced synthesis materials were investigated. For these purposes, the morphological effects of synthesis materials were examined by FTIR, XRD and SEM-EDX analyzes and their mechanical properties were investigated by hardness and compression tests.

As a result of FTIR and XRD investigations on all synthesized materials, it was observed that the additive materials decreased the crystallinity and formed the HA (Hydroxyapatite), β-TCP (Beta tricalcium phosphate), Ca<sub>3</sub>(Si<sub>3</sub>O<sub>9</sub>), Ca<sub>2</sub>H<sub>4</sub>O<sub>9</sub>P<sub>2</sub> phase structures. In addition, as a result of the SEM-EDX and mechanical tests, it has been determined that different sizes of grain structure in all synthesized materials are formed and SrBr<sub>2</sub> additive increase the compressive strength and hardness values.

**Keywords:** Calcium phosphate, SrBr<sub>2</sub>, Sol gel, Mechanical properties

## 1. Introduction

Recent studies have focused on the development of new types of biomaterials, with biological and mechanical properties similar to that of the human bone, by forging stronger chemical bonds between biomaterials and tissues to repair bone damage [1-8]. Bioceramics are of great interest because they are easy to produce and have a good biocompatibility. In addition to calcium phosphate compounds (hydroxyapatite, beta-tricalcium phosphate) used so far, alumina and zirconia have also been used as substitutes for hard tissues [9]. In addition to such compounds, bioceramics such as silicate-based wollastonite ( $\text{CaSiO}_3$ ) [10,11], dicalcium silicate ( $\text{Ca}_2\text{SiO}_4$ ) [12], bredigite ( $\text{Ca}_7\text{MgSi}_4\text{O}_{16}$ ) [13] and akermanite ( $\text{Ca}_2\text{MgSi}_2\text{O}_7$ ) [14] are preferred because of their excellent *in vitro* bioactivity, mechanical properties and biocompatibility. These compounds, also called biosilicates, play a crucial role in bone tissue engineering [15].

In mammalian bodies, elements such as Ca, Mg, and Si play a vital role in osteogenesis [15]. Calcium is an important element found in bones, teeth and skull and its deficiency causes various fatal diseases. Magnesium is required for bone growth, repair and maintenance and silicon is an essential element for skeletal development, and its deficiency can lead to skull deformation [16,17]. Biomaterials consisting of Ca, Mg and Si with low degradation have improved the mechanical properties significantly compared with conventional biomaterials such as calcium phosphate and calcium silicate [18].

Strontium (Sr) is a metal found in trace amounts in the bone structure. It has beneficial effects in both normal and diseased bone tissues [19]. Specifically, strontium ranelate has been identified as an effective compound in the medication used to reduce osteoporosis, as well as post-menopausal vertebral and hip fracture risk [20-22]. Moreover, Sr-containing silicates such as Sr-added  $\text{CaSiO}_3$  [23], strontium silicate ( $\text{SrSiO}_3$ ) [24] and Sr-containing bioglasses [25] have considerable effects on osteogenesis.

Overall, from the literature, it is concluded that there is not an optimal value for  $\text{SrBr}_2$  doping to meet the best morphological and mechanical behaviors. In the present study,  $\text{SrBr}_2$  was added into  $\text{Ca}(\text{NO}_3)_2 \cdot 4\text{H}_2\text{O}$ ,  $\text{SiO}_2$ ,  $\text{P}_2\text{O}_5$ ,  $\text{H}_3\text{BO}_3$ ,  $\text{MgO}$ ,  $\text{AgNO}_3$  based bone graft at different amounts by sol-gel method. Synthesis materials were produced by adding 5-20 wt%  $\text{SrBr}_2$ .

The morphological and mechanical effects of  $\text{SrBr}_2$  on synthesis material were investigated.

FTIR (Fourier-transform infrared spectroscopy), XRD (X-ray diffraction) and SEM-EDX (scanning electron microscopy-energy dispersive) analyses were used for the morphological properties while hardness and compression tests were performed to investigate mechanical properties.

## 2. Material ve Method

### 2.1. Material

In this study, powder chemical compounds, whose percentage by weight values are shown in Table 1, were dissolved in distilled water and ethanol and are produced by the sol gel method. As a chemical compound,  $\text{Ca}(\text{NO}_3)_2 \cdot 4\text{H}_2\text{O}$  (Sigma, Cas no:13477-34-4) powders were used as the primary components of the synthesis materials. As for the sintering additive,  $\text{SiO}_2$  (Sigma, Cas no:60676-86-0),  $\text{H}_3\text{BO}_3$  (Merck, Cas no: 10043-35-3),  $\text{MgO}$  (Tekkim, Cas no:191113.702),  $\text{P}_2\text{O}_5$  (97.1%purity, Merck-K33152940.418) and  $\text{AgNO}_3$  (99,99%purity, Sigma, Cas no: 7761-88-8) were used.  $\text{SrBr}_2$  (Alfa Aesar-10476-81-0) powders were added to all compounds in different ratios and their effects on the synthesis materials were investigated.

**Table 1.** Percentage by weight (%) values of the materials produced by sol-gel method

Sample code	$\text{Ca}(\text{NO}_3)_2 \cdot 4\text{H}_2\text{O}$	$\text{SiO}_2$	$\text{P}_2\text{O}_5$	$\text{H}_3\text{BO}_3$	$\text{MgO}$	$\text{AgNO}_3$	$\text{SrBr}_2$
CaMg0	45	40	5	5	-	5	-
CaMgSr1	35	30	5	10	10	5	5
CaMgSr2	30	30	5	10	10	5	10
CaMgSr3	30	20	5	10	10	5	20

### 2.2. Method

All chemical compounds except  $\text{P}_2\text{O}_5$  were first dissolved in ethanol, then magnetically stirred at 400 rpm for 30 min and finally mixed in an ultrasonic homogenizer at 37 °C for 30 min at 35% amplitude to obtain a homogenous solution. Although a magnetic stirrer is used to obtain the sol, a homogenizer is used for the homogenous dispersion and gelation of the particles. However,  $\text{P}_2\text{O}_5$  compound was dissolved in distilled water in a separate beaker and then added to the homogenizer to obtain the gel structure. After all, the synthesis materials had values below the pH value of 2, and the pH values were increased to 7.5 using NaOH solution without changing the gel structure of the solutions.

Synthesis materials aged 24 h in normal atmosphere were dried in the normal atmosphere at 120 °C for 24 h in an oven. For

FTIR and XRD analyses, the synthesis materials were sintered in powder form and while they were sintered as particles for SEM-EDX analyses. Moreover, after synthesis, to prepare the powder synthesis materials for mechanical tests, they were pressed under unidirectional isostatic press at a rate of 3 kN/s under a load of 30 N to have a cylindrical shape with a diameter of 15 mm and a height of 20 mm and then sintered under argon atmosphere for 3 h at 1050 °C. A tube furnace was used for sintering and temperature was increased to 1050 °C for approximately 3.5 h (5 °C/min), it was kept at 1050 °C for 3 h and temperature was decreased down to room temperature for 3.5 hours (5 °C/min).

### 2.3. Characterization

FTIR, XRD and SEM-EDX analyses were performed to investigate the microstructures and chemical properties of all the biomaterials produced by the sol gel method, while hardness and compression tests were conducted to examine their mechanical properties. Powder X-ray diffraction patterns of synthesis materials were obtained using X-ray diffractometer (BRUKER D8 ADVANCE) ( $\lambda = 1.5406\text{\AA}$ ), and diagrams were recorded at  $2\theta=0-90^\circ$  with a scan rate of  $2^\circ/\text{min}$  and the constant time interval of 1s.

FTIR (STI Unicam WATTSON 1000) analysis was performed to determine the structures of the synthesized samples. FTIR operating at 400-3200  $\text{cm}^{-1}$  wave range was used in the FTIR analyses, while SEM-EDX (JEOLJSM-7001F) instrument was used to investigate the morphological properties.

## 3. Results and Discussion

### 3.1. FTIR

Figure 1 shows the FTIR analysis results of all synthesis materials obtained between 3200 and 400  $\text{cm}^{-1}$ . According to the FTIR analysis results, all synthesis materials were determined to have similar peaks between 1087 and 400  $\text{cm}^{-1}$ . However, the following samples had different peaks: CaMg0 synthesis material at 1631  $\text{cm}^{-1}$ , CaMgSr1 synthesis material at 1380.4  $\text{cm}^{-1}$  and CaMgSr2 synthesis material at 1986.4 and 1380.0  $\text{cm}^{-1}$ . CaMg0 and CaMgSr2 synthesis materials formed H-OH bond (bending) at 1986.4 and 1631.0  $\text{cm}^{-1}$  peak magnitudes while

the Si-O-Si bond structure was formed at 1380.0 and 1380.04  $\text{cm}^{-1}$  peak magnitudes.

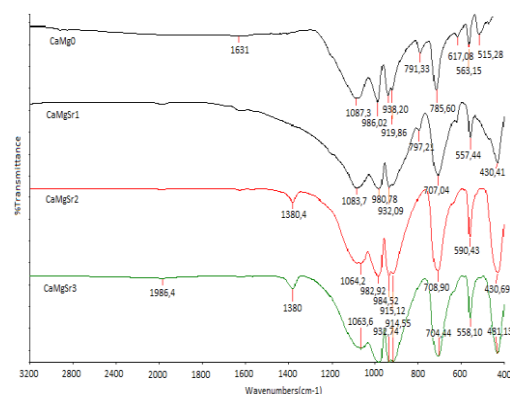


**Figure 1.** FTIR analysis results of CaMg0, CaMgSr1, CaMgSr2 and CaMgSr3 synthesis materials

H-OH and O-H peaks obtained at around 1640  $\text{cm}^{-1}$  indicate water absorbed in calcium silicate hydrate [26]. The bonds between 700 and 800  $\text{cm}^{-1}$  and the bonds close to 460  $\text{cm}^{-1}$  indicate vibration modes of Si-O-Si groups [27] while the peaks around 415  $\text{cm}^{-1}$  indicate O-Ca-O bending modes [28]. Moreover, the peaks between 400 and 800  $\text{cm}^{-1}$  indicate metal-oxygen stretching bonds [29,30]. Based on this information, the synthesis materials were found to give P-O-P vibration bands between 1087.3 and 914.55  $\text{cm}^{-1}$ , Si-O-Si and O-Si-O peaks between 797.21 and 515.28  $\text{cm}^{-1}$  and O-Ca-O vibration bands between 431.49 and 430.41  $\text{cm}^{-1}$ .

### 3.2. XRD

In many studies, HA and  $\beta$ -TCP phases have been observed depending on the sintering temperature and the materials added [31-34]. Even small amounts of  $\beta$ -TCP formation have been found to provide advantages such as increasing the bioactivity and ionic substitutions of the material [35]. Similar results were observed in materials containing  $\beta$ -CaSiO<sub>3</sub> and Ca<sub>3</sub>(Si<sub>3</sub>O<sub>9</sub>) containing phases and it was determined that the material can be used as a bone graft [36,37]. In our study, it was observed that the materials produced by obtaining HA,  $\beta$ -TCP and Ca<sub>3</sub>(Si<sub>3</sub>O<sub>9</sub>) phases gained similar advantages. According to all XRD analysis results obtained from all synthesis materials, the synthesis materials were observed to have similar peaks and the highest peak magnitude

was obtained in the CaMgO synthesis material, as shown in Figure 2a-d. Moreover, the main phase in all synthesis materials was HA while the

second phase was  $\text{Ca}_3(\text{Si}_3\text{O}_9)$  and also  $\beta$ -TCP and  $\text{Ca}_2\text{H}_4\text{O}_9\text{P}_2$  phases formed (Figure 2a-d).

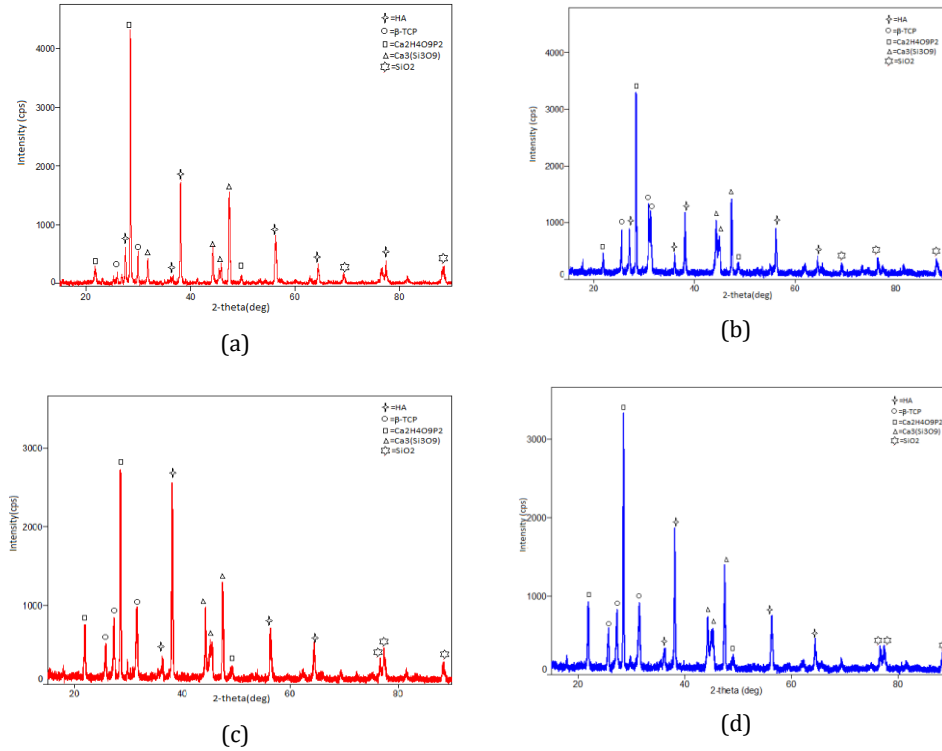
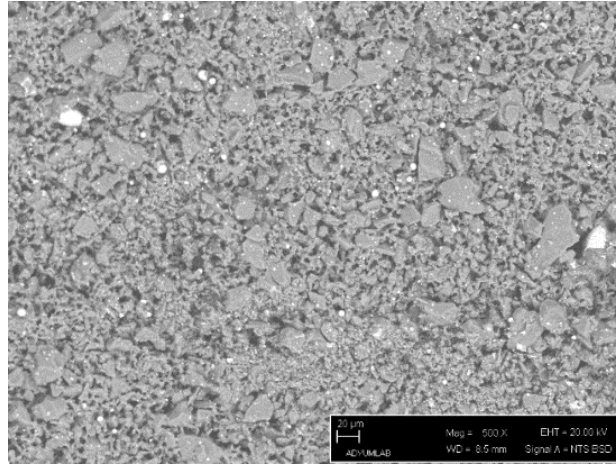


**Figure 2.** XRD analysis results: (a) CaMg0, (b) CaMgSr1, (c) CaMgSr2, (d) CaMgSr3

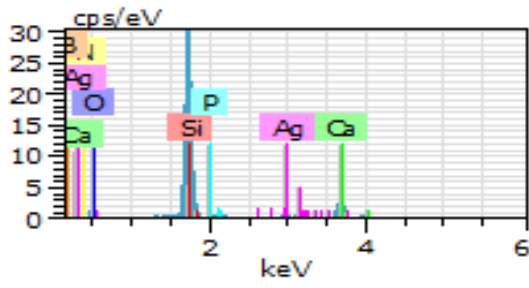
### 3.3. SEM-EDX

The main factors affecting and determining the stability of the material, sintering conditions and mechanical are the chemical composition, grain size and surface morphology of the material. Therefore,

Figures 3a-d, 4a-f and 5a-d show SEM-EDX images of synthesis samples at different magnifications produced by adding  $\text{SrBr}_2$  at 5 to 20 wt% into  $\text{Ca}(\text{NO}_3)_2 \cdot 4\text{H}_2\text{O}$ ,  $\text{SiO}_2$ ,  $\text{P}_2\text{O}_5$ ,  $\text{H}_3\text{BO}_3$ ,  $\text{MgO}$  and  $\text{AgNO}_3$  based synthesis materials.

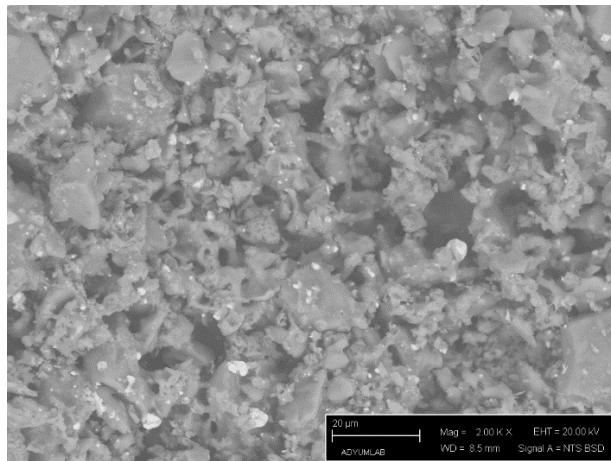


(a)

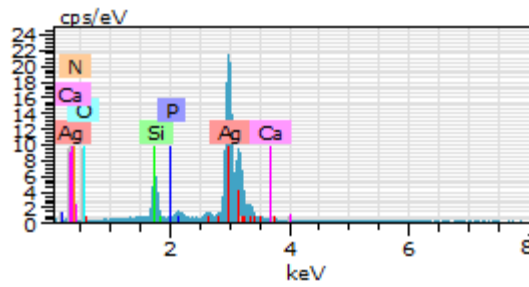


Element	Wt%	At%
Si	47.64	39.19
O	27.24	39.33
Ca	12.28	7.08
Ag	5.34	1.14
Br	3.83	8.18
N	2.60	4.28
P	1.07	0.80

(b)



(c)



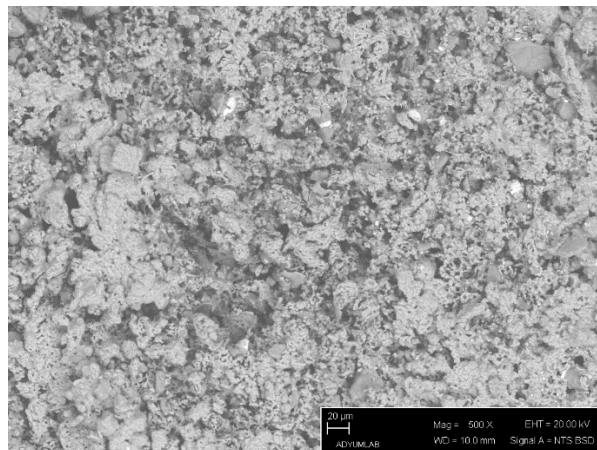
Element	Wt%	At%
Si	7.20	19.22
O	3.66	17.15
Ca	0.13	0.25
Ag	88.64	61.63
N	0.29	1.56
P	0.07	0.18

(d)

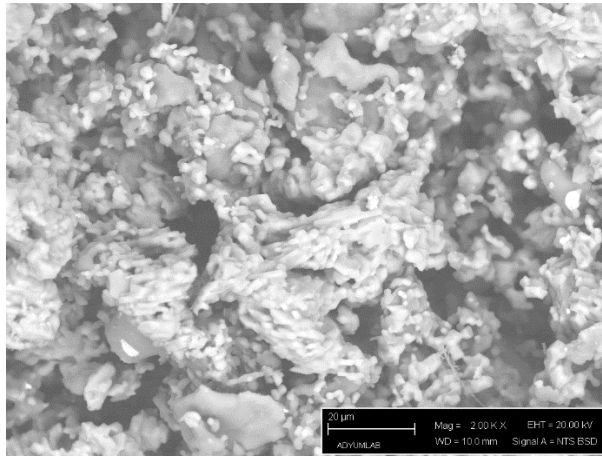
**Fig. 3.** SEM images of CaMgO synthesis material at different magnifications: (a) 500X, (c) 2000X and EDX results obtained from: (b) general view, (d) white particles on the surface

SEM images obtained from CaMgO synthesis material at 500X and 1000X magnifications indicate the formation of a morphological structures having different grain sizes and pore distribution, which shows the formation of grain distribution on the surface with different shapes and sizes (Figure 4a-b). EDX analysis results obtained from general surface view show that

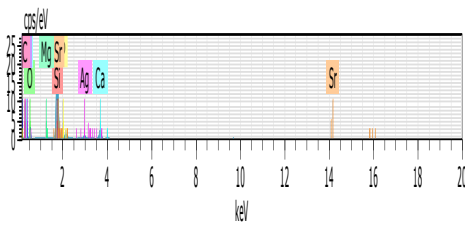
CaMgO synthesis material is composed of Ca, Si, B, O, Ag and N elements. Moreover, Figure 4c that the amounts of Si, Ca and O are high. EDX analysis result obtained from white grain structure formed on the surface indicates the formation of compounds with high amounts of Ag, Si and O.



(a)

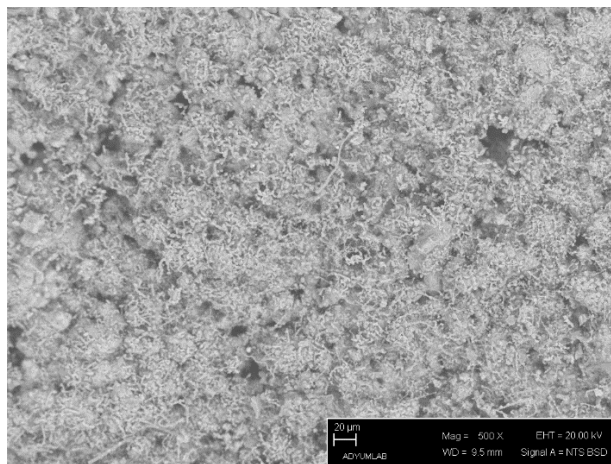


(b)

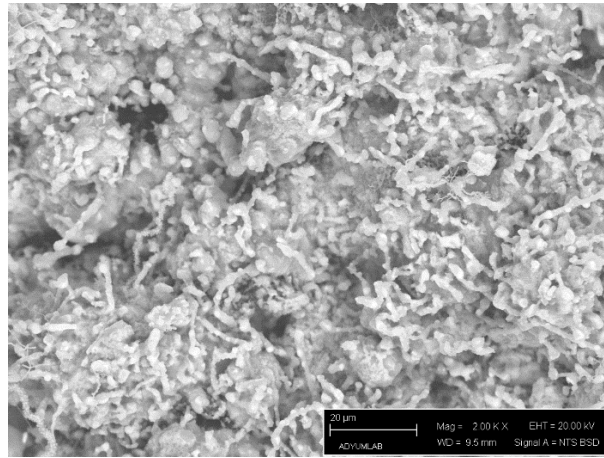


(c)

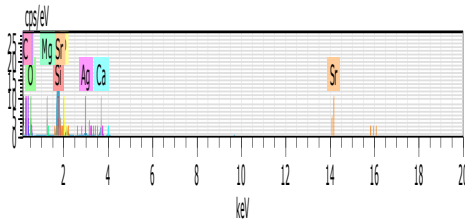
Element	Wt%	At%
Si	31.98	24.52
O	29.62	39.87
Ca	8.91	4.79
Ag	5.05	1.01
N	2.23	3.43
P	1.38	0.96
Br	2.09	4.16
Sr	1.38	0.96
Mg	0.94	0.83



(d)



(e)



(f)

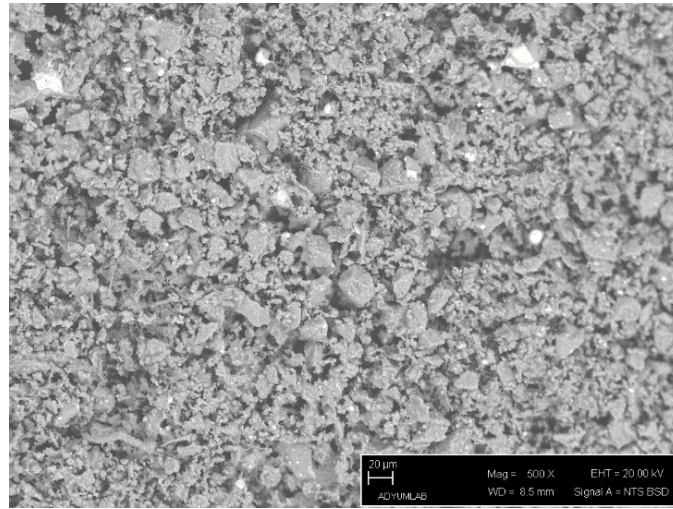
Element	Wt%	At%
Si	40.16	27.47
O	39.04	51.20
Ca	10.09	10.05
Ag	1.93	0.38
N	1.05	1.58
P	1.37	0.93
Br	4.01	7.78
Sr	2.23	0.53
Mg	0.11	0.10

**Figure 4.** SEM images of CaMgSr1 and CaMgSr2

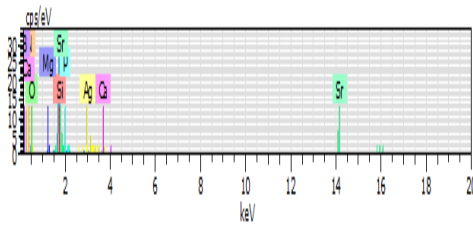
synthesis materials at different magnifications: (a,d) 500X and (b,e) 2000X and EDX results obtained from: (c) general view of CaMgSr1, (f) general view of CaMgSr2

SEM images obtained from SrBr<sub>2</sub> containing (5wt%-20wt%) CaMgSr1 and CaMgSr2 synthesis materials at different magnifications reveal the formation of a structure having different grain sizes and pore distribution, and they also show the formation of the structures agglomerated on the matrix surface, unlike CaMg0 synthesis material (Figure 4a-d). The grain size and the pore size and number

decreased with increasing amounts of SrBr<sub>2</sub>. Moreover, Figure 4a-d showed that when the amount of SrBr<sub>2</sub> was increased, there was a less agglomerated structure formed on the surface, and the grain sizes forming the agglomerate decreased. SEM images showed that liquid phase sintering was more pronounced in the CaMgSr2 synthesis material.

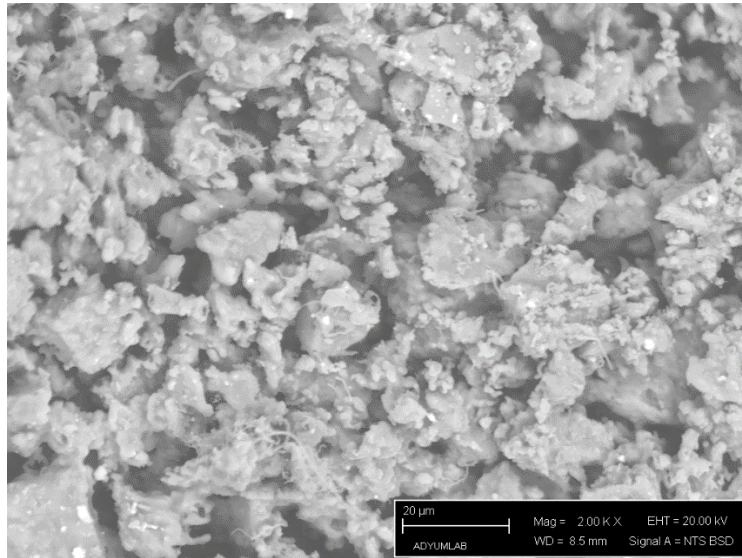


(a)

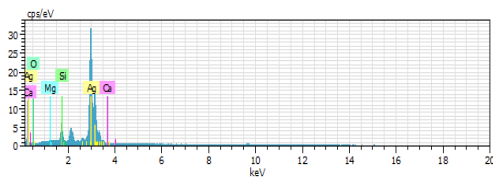


(b)

Element	Wt%	At%
Si	43.26	32.63
O	37.07	49.08
Ca	4.21	2.23
Ag	4.06	0.80
N	2.49	3.76
P	1.07	0.73
Br	4.74	9.29
Sr	1.96	0.47
Mg	1.15	1.00



(c)



(d)

Element	Wt%	At%
Si	3.04	7.37
O	8.50	36.17
Ca	0.28	0.48
Ag	88.01	55.52
Mg	0.16	0.46

**Figure 5.** SEM images of CaMgSr<sub>3</sub> synthesis materials at different magnifications: (a) 500X, (b) 2000X and EDX results obtained from: (c) general view, (d) white particles on the surface

SEM images of CaMgSr<sub>3</sub> synthesis material at 500X and 2000X magnifications showed that the appearance of the synthesis material was similar to the CaMgO synthesis material (Fig. 5a). Moreover, irregular surface morphology, agglomerated and pores at different sizes formed. Unlike CaMgSr<sub>1</sub> and CaMgSr<sub>2</sub> synthesis materials, Figure 5a-b showed that CaMgSr<sub>3</sub> with the highest SrBr<sub>2</sub> amount increased amount of pores due to the degree of liquid phase sintering decreased. Moreover, the amount of agglomerated structures formed on the surface of SrBr<sub>2</sub> containing synthesis materials was determined.

Figure 5d shows the EDX result obtained from CaMgSr<sub>3</sub> synthesis material, and also indicates that the synthesis material has a high amount of Si, O and B elements. The EDX result obtained from the agglomerated structure formed on the surface indicated that these structures have high amount of Ag, O and Si (Figure 5d).

In the SEM-EDX studies of calcium magnesium and silicate powders, the porous surface and agglomeration of the material is observed to help in cell viability and protein absorption [38]. In these materials used as biomaterials, it has been found that the porous and agglomerated surface causes positive interactions between the implant and surrounding tissue [39-42]. However, it has been determined that compounds containing Sr in calcium nitrate based biomaterials have positive effects not only on biocompatibility but also on biomaterials in terms of mechanical properties [43].

### 3.4. Mechanical Tests

If the natural healing process of the bone tissue is rapid and better under compressive loads, then the biomaterial should have a design to provide a proper compression [42]. Conversely, if the compression load is detrimental to wound healing, the opposite case may be followed. Unfortunately, the effects of compression or tensile loads on the long bone repair have not been fully understood [42]. Although the biomaterials available for defect repair are wide, during the development of a new biomaterial, factors such as biocompatibility, biodegradation, non-inflammation and having similar physical and mechanical properties to those of the bone should be considered by researchers and appropriate chemical compounds should be combined.

In another study on SrBr<sub>2</sub>, SrBr<sub>2</sub> effect was investigated by adding SrBr<sub>2</sub> to Ca (NO<sub>3</sub>)<sub>2</sub>·4H<sub>2</sub>O,

KOH, NaNO<sub>3</sub>, P<sub>2</sub>O<sub>5</sub>, and urea (CO (NH<sub>2</sub>)<sub>2</sub>). In addition, the morphological, mechanical and cytotoxicity effects of the porous structure formed by moving away from the structure with the effect of sintering temperature of urea was investigated. Thus, Studies performed on SrBr<sub>2</sub> have shown that the SrBr<sub>2</sub> compound and porous structure in bone injuries effects and enhances the mechanical properties of synthesis materials positively [43]. In our study, Ca(NO<sub>3</sub>)<sub>2</sub>·4H<sub>2</sub>O, SiO<sub>2</sub>, P<sub>2</sub>O<sub>5</sub>, H<sub>3</sub>BO<sub>3</sub>, MgO, AgNO<sub>3</sub>-based material were synthesized using the sol-gel method with some substitutions, such as SrBr<sub>2</sub>. As a result of the study, it was found that SrBr<sub>2</sub> helps to increase the morphological and mechanical properties of the synthesis materials.

#### 3.4.1. Hardness Test

Examination of the hardness values of synthesis materials, the lowest hardness was obtained in CaMgO, and the highest hardness was obtained in the CaMgSr<sub>3</sub> (Fig.6). It was determined as a result of investigations that SrBr<sub>2</sub> compound increased the hardness of synthesis materials and hardness values increased with increasing amounts of SrBr<sub>2</sub>.

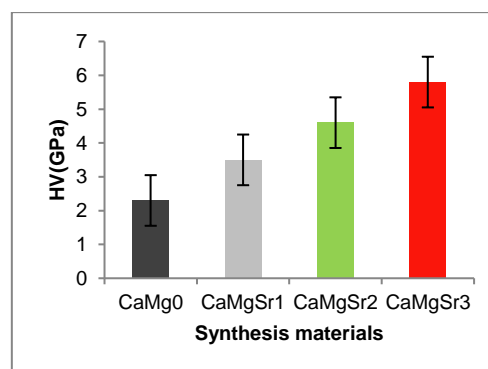
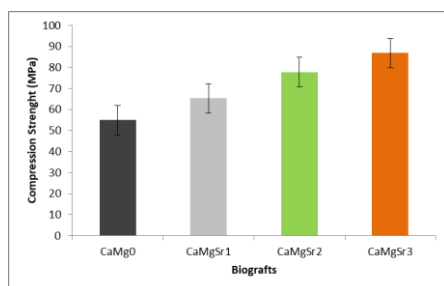


**Figure 6.** Vickers hardness values of CaMgO, CaMgSr<sub>1</sub>, CaMgSr<sub>2</sub> and CaMgSr<sub>3</sub> synthesis materials

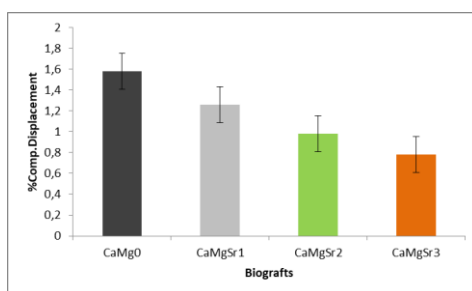
#### 3.4.2. Compression test

Studies performed on human bone showed that the cortical bone has strength of 100-150 MPa, trabecular bone has the strength of 2-12 MPa, and scaffolds have strength of 86±9 MPa [44-46]. The present study showed that the compression strength values of synthesis materials were between those of the cortical and trabecular bones. For example, the compressive strength of approximately 50% porous hydroxyapatite is 31 MPa [47]. Other values of compressive strengths are in the range 34-51 MPa [48-50]. SEM images

support these results, including the partial porous structure of synthesis materials and the compression strength values of synthesis materials, which were between those of cortical and trabecular bones.



(a)



(b)

**Figure7. (a)** Compression Strength and (b) %Compression Displacement values of CaMg0, CaMgSr1, CaMgSr2 and CaMgSr3 synthesis materials

Figure 7a-b shows compression strength and %compression displacement values obtained after compression tests of all synthesis materials. Compression strength and %compression displacement of synthesis materials showed that the lowest compressive strength was obtained in the CaMg0 and the highest compressive strength was achieved by the CaMgSr3 (Figure 7a). Moreover, %compression displacement values were inversely proportional to the compression strength values and the highest values were obtained from CaMg0 and the lowest values were obtained from CaMgSr3 synthesis materials. Thus, it was determined that the SrBr<sub>2</sub> compound increased the compressive strength value of the synthesis materials and the compression strength increased with the increasing amounts of SrBr<sub>2</sub>. In this study, the

results of the analysis support each other and in the FTIR analysis results, the increase in peak intensity due to the increase in SrBr<sub>2</sub> amount increased the crystallinity. For this reason, it was determined that Compression Strength and hardness values increased together with the increase in crystallinity. Also, at SEM images, pore amount of materials together with increased SrBr<sub>2</sub> amount decreased but liquid phase sintering in the structure increased. However, decreased pore density of materials caused an increase in both the Compression Strength and hardness

## CONCLUSION

The present study evaluated the chemical, morphological and mechanical properties of Ca(NO<sub>3</sub>)<sub>2</sub>·4H<sub>2</sub>O, SiO<sub>2</sub>, P<sub>2</sub>O<sub>5</sub>, H<sub>3</sub>BO<sub>3</sub> and AgNO<sub>3</sub> based and SrBr<sub>2</sub> added synthesis materials produced by the sol-gel method.

- FTIR and XRD analysis results showed that the sharpest peaks were obtained from the CaMg0 synthesis material among all synthesis materials and the highest peak magnitude was obtained from CaMgSr3 synthesis material among SrBr<sub>2</sub> containing synthesis materials. Thus, the synthesis material with the highest crystalline structure was CaMg0 while CaMgSr3 showed the highest crystalline structure among the SrBr<sub>2</sub> containing synthesis materials. FTIR analyses showed that in addition to OH<sup>-</sup> peaks, the peaks related to (PO<sub>4</sub>)<sup>-3</sup> and M-O compounds were formed. XRD analyses showed that in all synthesis materials, except HA and β-TCP phases, Ca<sub>3</sub>(Si<sub>3</sub>O<sub>9</sub>) and SiO<sub>2</sub> compounds were formed.

- As a result of SEM image analysis results performed for morphological investigations, it was determined in all synthesis materials that different grain sizes and pore distribution were observed while in SrBr<sub>2</sub> containing synthesis materials, the number of pores decreased and agglomerated grain structure formed on the matrix structure.

- Evaluation of the compressive strength and hardness values of all synthesis materials showed that SrBr<sub>2</sub> compound increased compressive strength and hardness values and the highest mechanical values were achieved by the CaMgSr3 synthesis material.

- The highest mechanical values were found for the CaMgSr3 biograft, which, having the lowest

porosity, suggests that the mechanical values also increases in low-porous grafts.

- From the overall results, considering the mechanical properties and structure tests together, the synthesized biograft CaMgSr3 provided better correlation between morphological and mechanical property.

## References

- [1] Liang, W., Rahaman, M. N., Day, D. E., Marion, N. W., Riley G. C., Mao J. J., 2008. Bioactive borate glass scaffold for bone tissue engineering, *J. Non-Cryst. Solids*, Volume. 354, p.1690-1696.
- [2] Mariappan, C.R., Yunos, D. M., Boccaccini, A. R., Roling, B., 2009. Bioactivity of electro-thermally poled bioactive silicate glass, *Acta Biomater.*, Volume. 5 [4], p.1274-1283.
- [3] Ouis, M. A., Abdelghany, A. M., Elbatal, H. A., 2012. Corrosion mechanism and bioactivity of borate glasses analogue to Hench's bioglass, *Processing and Application of Ceramics*, Volume. 6 [3], p.141-149.
- [4] Jha, P. and Singh, K., 2016. Effect of MgO on bioactivity, hardness, structural and optical properties of SiO<sub>2</sub>-K<sub>2</sub>O-CaO-MgO glasses. *Ceramics International*, 42(1), p.436-444.
- [5] Esmati, N., Khodaei, T., Salahinejad, E. and Sharifi, E., 2018. Fluoride doping into SiO<sub>2</sub>-MgO-CaO bioactive glass nanoparticles: bioactivity, biodegradation and biocompatibility assessments. *Ceramics International*, Volume 44(14), p.17506-17513.
- [6] Arabyazdi, S., Yazdanpanah, A., Hamedani, A.A., Ramedani, A. and Moztafzadeh, F., 2019. Synthesis and characterization of CaO-P<sub>2</sub>O<sub>5</sub>-SiO<sub>2</sub>-Li<sub>2</sub>O-Fe<sub>2</sub>O<sub>3</sub> bioactive glasses: The effect of Li<sub>2</sub>O-Fe<sub>2</sub>O<sub>3</sub> content on the structure and in-vitro bioactivity. *Journal of Non-Crystalline Solids*, Volume 503, p.139-150.
- [7] Ma, J., Huang, B.X., Zhao, X.C., Wang, C.Z. and Zhang, H.M., 2017. Effect of zinc substitution for calcium on the structure, dissolution behavior and apatite formation of CaO-ZnO-SiO<sub>2</sub>-P<sub>2</sub>O<sub>5</sub> bioceramics. *Materials Letters*, Volume 206, p.154-157.
- [8] Ke, D., Tarafder, S., Vahabzadeh, S. and Bose, S., 2019. Effects of MgO, ZnO, SrO, and SiO<sub>2</sub> in tricalcium phosphate scaffolds on in vitro gene expression and in vivo osteogenesis. *Materials Science and Engineering: C*, Volume 96, p.10-19.
- [9] Hench, L.L., 1991. Bioceramics: From Concept to Clinic, *J. Am. Ceram. Soc.*, Volume. 74, p.1487-1510.
- [10] Deaza, P. N., Guitian, F., Deaza, S., 1994. Bioactivity of Wollastonite Ceramics: In Vitro Evaluation, *Scr. Metall. Mater.*, Volume. 31, p. 1001-1005.
- [11] Lin, K. L., Zhai, W. Y., Ni, S. Y., Chang, J., Zeng, Y., Qian, W. J., 2005. Study of the Mechanical Property and in vitro Biocompatibility of CaSiO<sub>3</sub> Ceramics, *Ceram. Int.*, Volume. 31, p. 323-326.
- [12] Gou, Z. R., Chang, J., Zhai, W. Y., 2005. Preparation and Characterization of Novel Bioactive Dicalcium Silicate Ceramics, *J. Eur. Ceram. Soc.*, Volume. 25, p. 1507-1514.
- [13] Wu, C. T., Chang, J., Wang, J. Y., Ni, S. Y., Zhai, W. Y., 2005. Preparation and characteristics of a calcium magnesium silicate (bredigite) bioactive ceramic, *Biomaterials*, Volume. 26, p.925-2931.
- [14] Wu, C. T., Chang, J., 2006. A novel akermanite bioceramic: preparation and characteristics, *J. Biomater. Appl.*, Volume. 21, p.119-129.
- [15] Choudhary, R., Koppala, S., Swamiappan, S., 2015. Bioactivity studies of calcium magnesium silicate prepared from eggshell waste by sol-gel combustion synthesis, *Journal of Asian Ceramic Societies*, Volume. 3-2, p.173-177.
- [16] Liu, C. C., Yeh, J. K., Aloia, J. F., 1988. Magnesium directly stimulates osteoblast proliferation, *J. Bone Miner. Res.*, Volume. 3, p. 104.
- [17] Carlisle, E. M., 1980. Biochemical and morphological changes associated with long bone abnormalities in silicon deficiency, *J. Nutr.*, Volume. 110, p. 1046-1055.
- [18] Wu, C., Chang, J., 2007. Degradation, bioactivity, and cytocompatibility of diopside, akermanite, and bredigite ceramics, *J. Biomed. Mater. Res. Part B*, p.153-160.
- [19] Marie, P. J., Ammann, P., Boivin, G., Rey, C., 2001. Mechanisms of action and therapeutic potential of strontium in bone, *Calcif. Tissue Int.*, Volume. 69, 121-129.
- [20] Meunier, P.J., Roux, C., Seeman, E., Ortolani, S., Badurski, J. E., Spector, T. D., et al., 2004. The effects of strontium ranelate on the risk of vertebral fracture in women with postmenopausal osteoporosis, *N. Engl. J. Med.*, Volume. 350, p. 459-468.
- [21] Fardellone, P., et al. 2005. Strontium ranelate reduces the risk of vertebral fractures in osteoporotic postmenopausal women whatever the baseline vertebral fracture status, *Bone*, Volume. 36, p. 403.
- [22] Reginster, J. Y., et al., 2005. Strontium ranelate reduces the risk of nonvertebral fractures in postmenopausal women with osteoporosis: Treatment of Periphraseal Osteoporosis (TROPOS) study, *The journal of clinical endocrinology & metabolism*, Volume. 90 [5], p. 2816-2822.
- [23] Chengtie, W., et al., 2007. The effect of strontium incorporation into CaSiO<sub>3</sub> ceramics on their physical and biological properties, *Biomaterials*, Volume. 28 [21], 3171-3181.
- [24] Zhang, M., et al., 2010. Synthesis, in vitro hydroxyapatite forming ability, and cytocompatibility of strontium silicate powders, *Journal of Biomedical Materials Research Part B: Applied Biomaterials*, Volume. 93[1], p.252-257.
- [25] Gentleman, E., et al., 2010. The effects of strontium-substituted bioactive glasses on osteoblasts and osteoclasts in vitro, *Biomaterials*, Volume. 31[14], p.3949-3956.
- [26] Park, J., Lakes, S.R., 1992. *Biomaterials: An Introduction*, Plenum Press, New York, p. 235.
- [27] Lopes M.A., Santos J.D., Monteiro F.J., Knowles J.C., 1998. Glass-reinforced hydroxyapatite: a comprehensive study of the effect of glass composition on the crystallography of the composite. *J Biomed. Mater. Res.*, Volume 39, p. 244-251.
- [28] Knowles J.C., 1993. *Ceramic Industry Division Annual Convention*. Brunel University, p. 20-23.
- [29] Sylvester P.W., Birkenfeld H.P., Hosick H.L., Briski K.P., 1994. Fatty acid modulation of epidermal growth factor-induced mouse mammary epithelial cell proliferation in vitro. *Exp Cell Res.*, Volume 214, p. 145-153.

- [30] Legeros R.Z., 1991. Calcium phosphates in oral biology and medicine. Monograph in Oral Sci., Volume 15, p. 1-201.
- [31] Nita S., Michel A., 2005. Cyclic silicate active site and stereochemical match for apatite nucleation on pseudowollastonite bioceramic-bone interfaces. *Biomaterials*, Volume 26, p. 5763-5770.
- [32] Hamisah I., Roslinda S., Hamid Muhammad A.A., 2016. Effect of autoclaving and sintering on the formation of  $\beta$ -wollastonite. *Mater. Sci. Eng. C*, Volume 58, p.1077-1081.
- [33] Paital, S.R. and Dahotre, N.B., 2009. Calcium phosphate coatings for bio-implant applications: materials, performance factors, and methodologies. *Materials Science and Engineering: R: Reports*, Volume 66(1-3), pp.1-70.
- [34] Saiz, E., Goldman, M., Gomez-Vega, J.M., Tomsia, A.P., Marshall, G.W. and Marshall, S.J., 2002. In vitro behavior of silicate glass coatings on Ti6Al4V. *Biomaterials*, Volume 23(17), pp.3749-3756.
- [35] Montenero, A., Gnappi, G., Ferrari, F., Cesari, M., Salvioli, E., Mattogno, L., Kaciulis, S. and Fini, M., 2000. Sol-gel derived hydroxyapatite coatings on titanium substrate. *Journal of Materials science*, Volume 35(11), pp.2791-2797.
- [36] Lakshmi, R., Velmurugan, V. and Sasikumar, S., 2013. Preparation and phase evolution of Wollastonite by sol-gel combustion method using sucrose as the fuel. *Combustion Science and Technology*, Volume 185(12), pp.1777-1785.
- [37] Martinez, I. M., Velasquez, P. A., Meseguer-Olmo, L., De Aza, P. N., 2011. Production and study of in vitro behaviour of monolithic  $\alpha$ -Tricalcium Phosphate based ceramics in the system  $\text{Ca}_3(\text{PO}_4)_2$ - $\text{Ca}_2\text{SiO}_4$ . *Ceram. Int.*, Volume. 37, p.2527-2535.
- [38] Zuleta, F., Murciano, A., Gehrke, S. A., E.Maté-Sánchez de Val, J., Calvo-Guirado, J. L., De Aza, P. N., 2017. A New Biphasic Dicalcium Silicate Bone Cement Implant, *Materials*, Volume. 10[7], p.758.
- [39] Choudhary, R., Koppala, S., Swamiaappan, S., 2015. Bioactivity studies of calcium magnesium silicate prepared from eggshell waste by sol-gel combustion synthesis, *Journal of Asian Ceramic Societies*, Volume. 3, p.173-177.
- [40] Ayala, A., Fetter, G., Palomares, E., Bosch, P., 2011. CuNi/Al hydrotalcites synthesized in presence of microwave irradiation, *Mater. Lett.*, Volume. 65, p.1663-1665.
- [41] Abdelkader, N. B. H., Bentouami, A., Derriche, Z., Bettahar, N., De Menorval, L. C., 2011. Synthesis and characterization of Mg-Fe layer double hydroxides and its application on adsorption of Orange G from aqueous solution, *Chem. Eng. J.*, Volume. 169, p. 231-238.
- [42] Park, J. B., 1979. *Biomaterials An Introduction*, 46-75p., New York.
- [43] Demirel, M., Aksakal, B., Kaya, A.I., 2017. The effect and characterization of newly synthesized SrBr<sub>2</sub> reinforced bone grafts on structure and cell viability, *Journal of Sol-Gel Science and Technology*, Volume. 82[2], p. 602-610.
- [44] Liu, X., Rahaman, M. N., Hilmas, G. E., Bal, B.S., 2013. Mechanical properties of bioactive glass (13-93) scaffolds fabricated by robotic deposition for structural bone repair, *Acta biomaterialia*, Volume. 9[6], p. 7025-7034.
- [45] Fu, Q., Saiz, E., Rahaman, M. N., Tomsia, A. P., 2011. Bioactive glass scaffolds for bone tissue engineering: state of the art and future perspectives, *Mater. Sci. Eng. C*, Volume. 31, p. 1245-56.
- [46] Lewandrowski, K.U., Wise, D. L., Yaszemski, M.J., Gresser, J. D., Trantolo, D. J., Altobelli, D. E., 2002. *Tissue engineering and biodegradable equivalents, scientific and clinical applications*, Marcel Dekker Inc., New York, NY.
- [47] Brown, W.E., 1987. A new calcium phosphate, water-setting cement. *Cements research progress*, pp.351-379.
- [48] Chow, L.C., 1991. Self-setting calcium phosphate cements. In *Mat Res Soc Symp Proc*. Volume 179, pp. 3-24.
- [49] Fukase, Y., Eanes, E.D., Takagp, S., Chow, L.C. and Brown, W.E., 1990. Setting reactions and compressive strengths of calcium phosphate cements. *Journal of dental research*, Volume 69[12], pp.1852-1856.
- [50] Takezawa, Y., Doi, Y., Shibata, S., Wakamatsu, N., Kamemizu, H., Goto, T., Iijima, M., Moriwaki, Y., Uno, K., Kubo, F. and Haeuchi, Y., 1987. Self-setting apatite cement. II. Hydroxyapatite as setting accelerator. *J. Jpn. Soc. Dent. Mat*, Volume 6, pp.426-431.